Cassiterite Fingerprinting

An overview of source and system characterisation via minor and trace element substitution mechanisms

Jason M. Bennett[1], Anthony I. S. Kemp[1], Marco L. Fiorentini[1], Steffen G. Hagemann[1], Malcolm P. Roberts[2]

[1]Centre for Exploration Targeting, School of Earth Sciences, University of Western Australia, Australia

[2]Centre for Microscopy, Characterisation and Analysis, University of Western Australia, Australia

THE UNIVERSITY OF WESTERN AUSTRALIA

Centre for EXPLORATION TARGETING

Cassiterite: the critical metals connection

The emerging technologies of the 21st Century require various metals that are termed 'critical' or 'strategic' by various world government/industry bodies. Geoscience Australia (Skirrow et al., 2013) classifies **Li, Nb, Ta, W, In,** Ga, Mo, Sb, Cr, Mn, Mg, Ni, Co, V, Te, the Rare Earth Elements (REEs) and the Platinum Group Elements (PGEs) as 'category one' critical commodities. Many of these metals (highlighted in bold) are intimately assoicated with **Sn**, itself a 'category two' critical commodity with **Ti, Be, Zr, Bi, F,** Se, Sr, Ge, Zn and C (as graphite).

Many of these elements do not occur in sufficient concentrations on their own to form economically viable deposits, but are instead extracted as by-products of other base metals, such as Sn, Pb, Cu and Zn. In Figure 1, these associations are graphically displayed as a 'wheel of companionality' (Nassar et al., 2015). A further commonality to these deposits is their relation in some way to granitic magmas. Figure 2 illustrates a schematic physicochemical model showing an idealised relationship between deposit types such as Li-Sn-Ta-(Nb) pegmatites, Sn-Cu-Pb-Zn skarns, and Sn-W-(Bi) hydrothermal vein and greisen deposits (Taylor, 1979; Lehmann, 1990; Lehmann, 2020). Despite the different controls on mineralisation for each of these deposits (silicate vs aqueous fluids), Sn is precipitated dominantly as cassiterite (SnO_2).

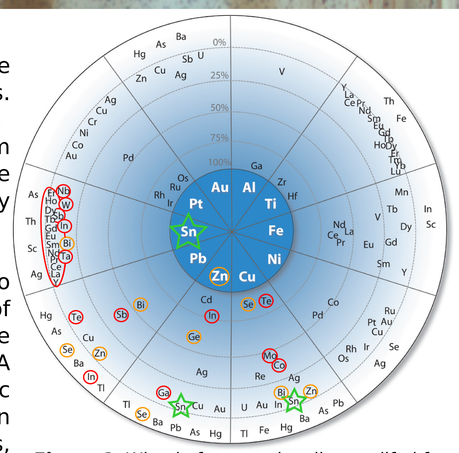

***Figure 1**: Wheel of companionality modifed from Nassar et al. (2015) to highlight category one and category two critcal metals (Skirrow et al., 2013) associated with Sn-bearing mineral systems.*

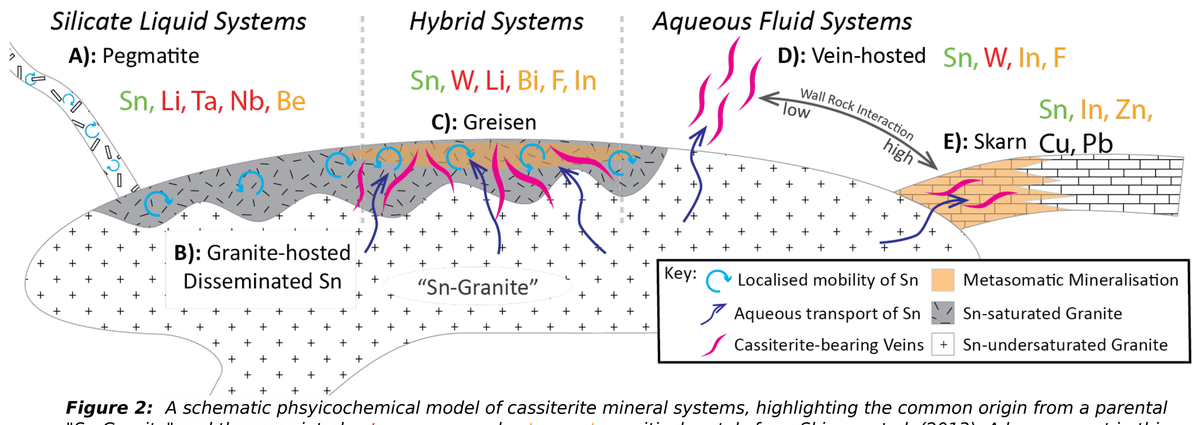

***Figure 2:** A schematic phsyicochemical model of cassiterite mineral systems, highlighting the common origin from a parental "Sn-Granite" and the associated category one and category two critical metals from Skirrow et al. (2013). A key concept in this model is that cassiterite precipitates under: 1. Dominantly magmatic conditions in* Silicate Liquid Systems *such as Pegmatites (A) and Granite-hosted Disseminated Sn deposits (B); 2. A* Hybrid *of magmatic-hydrothermal conditions in deposit classes such as Greisens (C); or as purely* Aqueous Fluid *derived deposit classes such as Vein-hosted (D) or Skarn (E) systems.*

Growth microstructures: a record of dynamic mineralisation processes

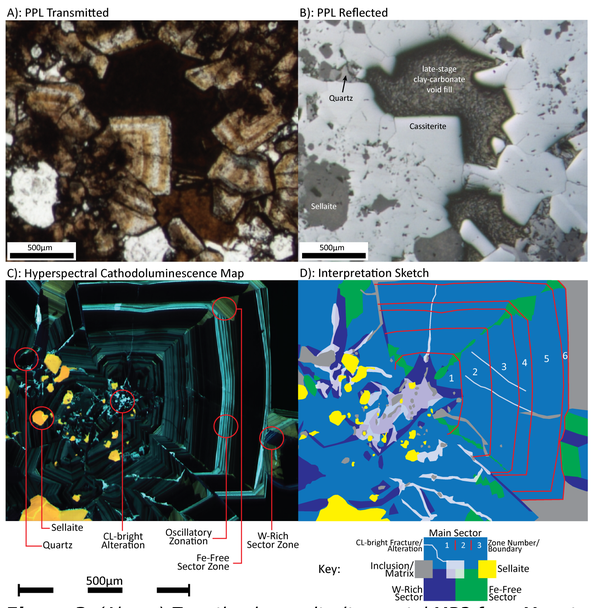

***Figure 3**: (Above) Zonation in cassiterite crystal MB3 from Mount Bischoff, Tasmania. (A) Transmitted PPL (B) Reflected PPL (C) false coloured Hyperspectral CL, bins R=600-900 nm, G=500-600, B=200-500 nm. (D) Interpretation sketch. Distinct concentric growth zones in the {100} sector are annotated 1 through 6.*

***Figure 4**: (Right) Paragenetic summary diagram for MB3 across the {100} sector concentric zonation. The normalised trace element concentrations are visually estimated from the count maps presented in Figures 6-8. The optical colour profile generally correlates with mean trace element abundance, and the CL brightness is inversely correlated with mean trace element content.*

Optical imaging, hyperspectral cathodoluminescence, X-ray element, and laser ablation trace element mapping reveal concentric growth zones and oscillatory zonation, sector growth zones, and secondary alteration features in cassiterite crystals. The minor elements Ti, Fe, Nb, Ta and W all exhibit concentric growth banding behaviour, which is mirrored in the trace elements Mn, Zr, Hf, Al, Sc, Sb, Ga, V, In, Mo, Y and U in LA-ICP-MS element maps.

The X-ray element maps show that there are two different CL-dark sector zones that correspond to separate growth faces of a cassiterite crystal, an Fe-rich {100} sector and a W-rich {101} sector. The CL-bright {110} sectors are relatively W- and Fe-poor. These sector zones affect elements where substitution occurs via charge-balanced coupled substitution.

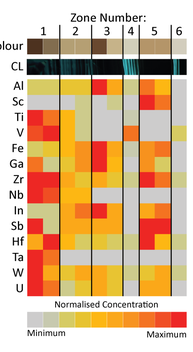

In-situ cassiterite geochemistry data must therefore be considered carefully. The combination of concentric and sector zonation microstructures result in multimodal element distributions, often strong enough to have the appearance of an on/off effect (such as seen in W). Averages are in effect 'mean'-ingless, instead X-ray element maps or LA-ICP-MS trace element maps are the best mechanisms to report the internal composition of cassiterite crystals.

Systematic trends in substitution mechanisms

Despite the internal chemical variability within single cassiterite crystals, there are clear chemical differences between the different paragenetic settings identified in Figure 2. This is exploitable in a Ti-(Fe,Mn)-(Nb,Ta) ternary diagram as in Figure 9. The uptake of these minor elements into the cassiterite lattice are controlled by charge-balanced coupled substituion mechanisms that differ in their dominance between crystals that precipitated from pegmatite-, greisen-, vein- or skarn-hosted systems. The overall concentration of each element also requires careful consideration - the overlapping areas of pegmatite and greisen systems are distinguished by much higher concentrations in pegmatitic cassiterite for instance, and very low totals of substituting elements plot with considerable scatter.

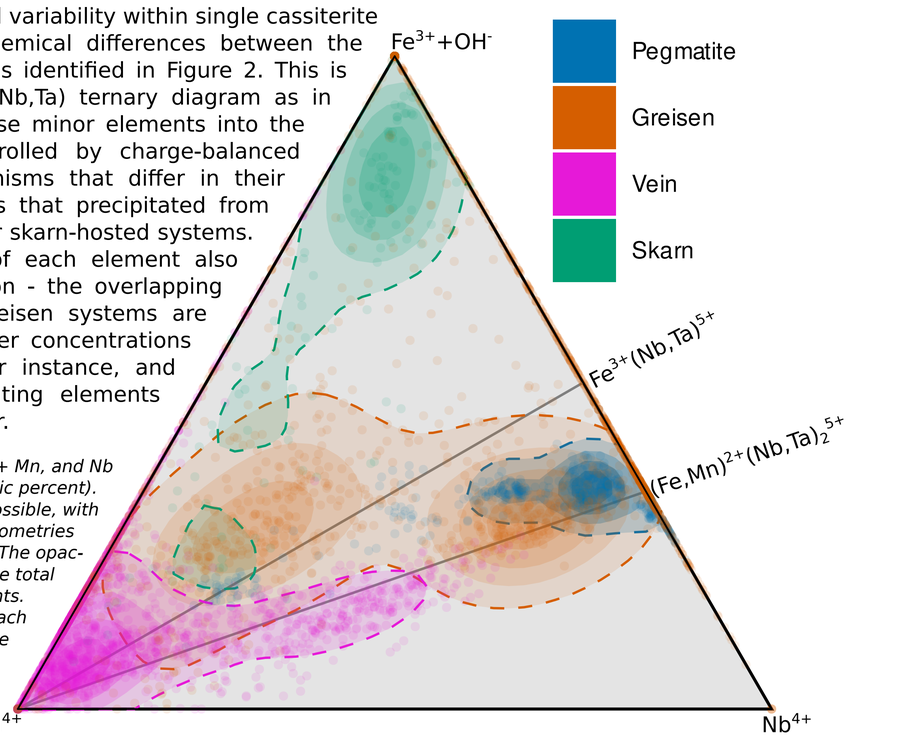

***Figure 9:** Ternary plot of the Ti, Fe + Mn, and Nb + Ta contents of cassiterite (in atomic percent). Five substitution mechanisms are possible, with tie lines between 1:1 and 2:1 stoichiometries joined to the Ti apex shown in grey. The opacity of each point is determined by the total concentration of substituting elements. Probability density estimations for each class are also shown, highlighting the distinct distributions of cassiterite composition as a function of mineralisation environment.*

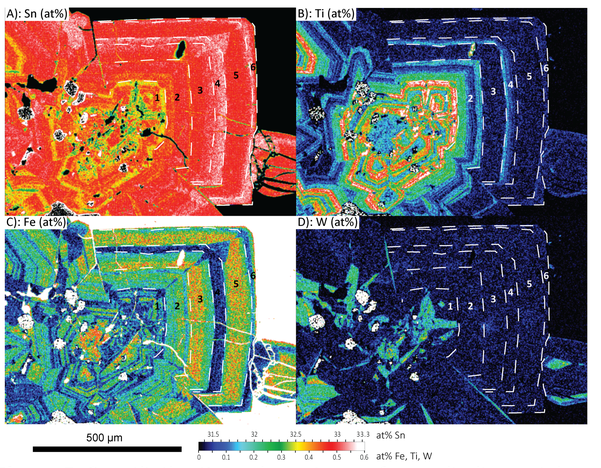

***Figure 5**: Quantitative X-ray element maps for cassiterite crystal MB3. (A) Sn. (B) Ti. (C) Fe. (D) W. Sector zonation is displayed by W and Fe, but not by Ti. All elements are concentrically zoned.*

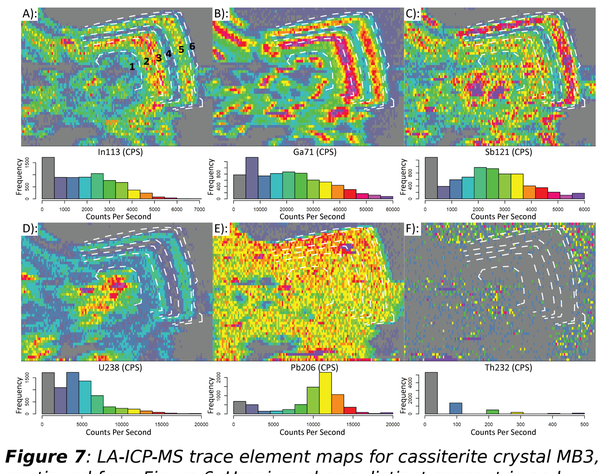

***Figure 7**: LA-ICP-MS trace element maps for cassiterite crystal MB3, continued from Figure 6. Uranium shows distinct concentric and sector zonation, supporting the incorporation of U into the cassiterite lattice. Thorium is not detected throughout most of the crystal.*

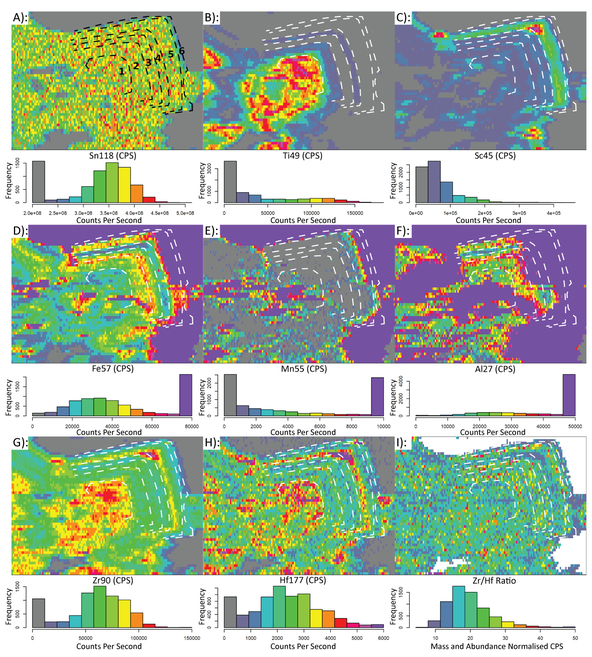

***Figure 6**: LA-ICP-MS trace element maps for cassiterite crystal MB3. Ablation transects start at the bottom right corner and proceed right to left on each row. All maps are background corrected counts per second (CPS). Dashed lines represent concentric zonation boundaries from Figure 3. Colour scale for each map is presented as a frequency histogram. The Fe, Mn and Al maps are smeared due to the composition of the late-stage void fill.*

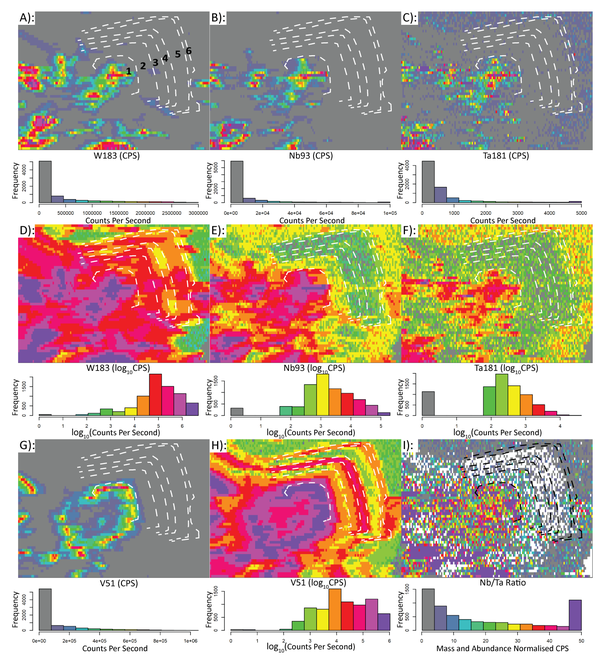

***Figure 8**: LA-ICP-MS trace element maps for cassiterite crystal MB3, continued from Figures 6 and 7. The concentric zonation in W, Nb and Ta is obscured by sector zonation on a linear scale, but is illuminated under a log_{10} transformation. The concentric zonation in V also requires a log_{10} scale to see the zonation clearly. Distinct zonation in the Nb/Ta ratio differs from the Zr/Hf ratio observed in Figure 6i when measurable (white areas denote NaN values, i.e., division by 0).*

Cassiterite grains from Silicate Liquid Systems are also readily distinguished from those precipitated in Aqueous Fluid Systems by their Nb/Ta and Zr/Hf ratios (Figure 10). The Nb/Ta and Zr/Hf ratios of granitic magmas evolve from narrowly constrained chondritic (⊙) and continental crust (♁) values (stage 1) through fractional crystallisation processes (stage 2) to variable low Nb/Ta and Zr/Hf ratios of 'rare metal granites' (stage 3). Most greisen (granite-hosted) cassierite crystals plot at this stage. Further fractional crystallisation processes lead to extreme low Nb/Ta and Zr/Hf ratios as recorded in cassiterites from pegmatites (stage 4a), or to extreme high Nb/Ta and a return towards crustal/chondritic Zr/Hf ratios in hydrothermal cassiterites (stage 4b).

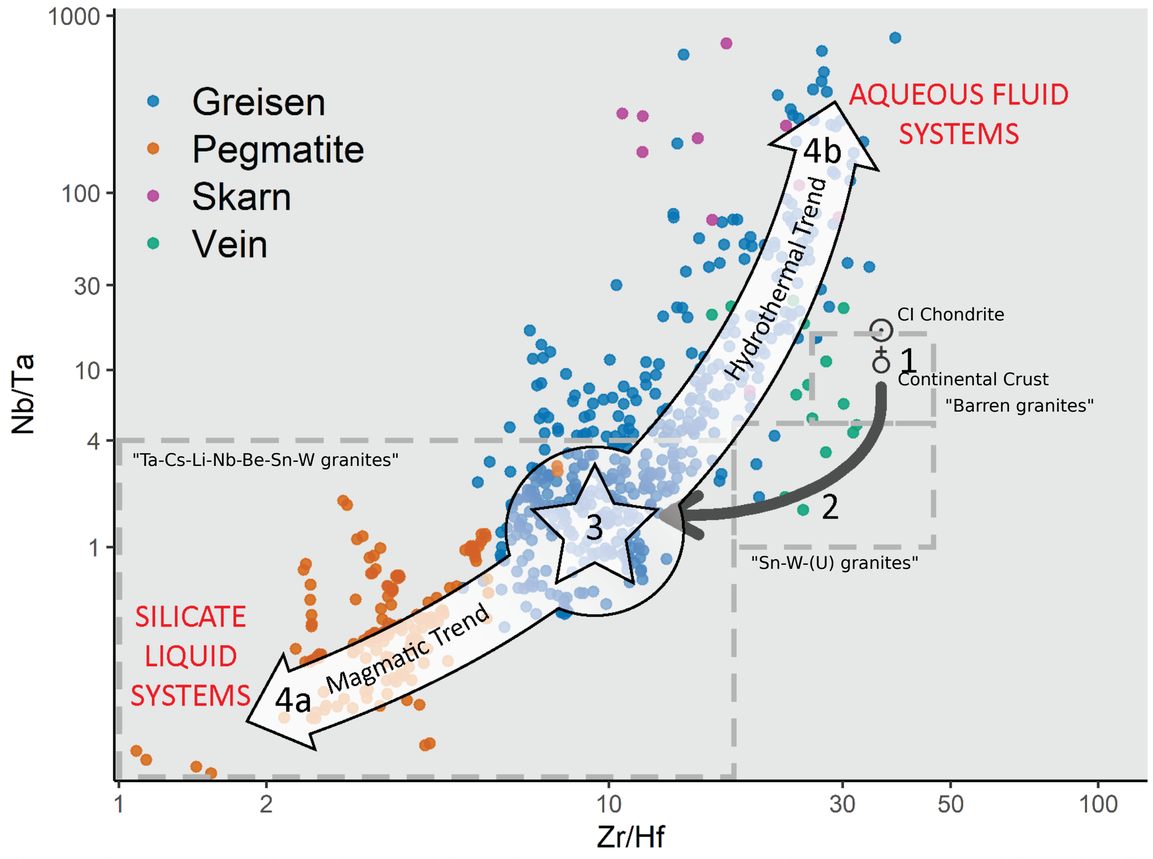

***Figure 10**: The 4-stage evolutionary history of Nb/Ta and Zr/Hf ratios observed in cassiterite. Values for the parental granitic melt start at **1** (the bulk continental crust, ♁), evolving via fractional crystallisation (**2**) to values typical of a 'Sn-granite' (**3**). Further fractionation towards extremely low values is observed in cassiterite from Silicate Liquid Systems (**4a**), whereas fractionation towards extremely high Nb/Ta is observed in cassiterite crystals from Aqueous Fluid Systems (**4b**). The grey dashed boxes represent the fields for 'Barren', 'Sn-W-(U)', and 'Ta-Cs-Li-Nb-Be-Sn-W' granites of Ballouard et al. (2016).*

Further analyses of cassiterite crystals across a single deposit and vein system will allow for the tracking of growth zone chemistry throughout the deposit, and determine if the movement of certain metals of interest (such as W or In) may be traced from source to sink. This would allow for the development of better exploration tools for Sn and other 'critical' metals. This work, in addition to discrimination into more nuanced deposit styles with a larger list of trace elements (such as including Al, Sc, Sb, Ga, V, In, Mo, Y and U) utilising statistical data mining methods, is the focus of current and future research.

Further Details

Bennett, J. (2021). *On the Geochemistry of Cassiterite.* [Doctoral Thesis, The University of Western Australia].

DOI: 10.26182/d6ad-7h10 | UWA Research Profile | Google Scholar Profile

References:
Ballouard, C. et al. (2016) 'Nb-Ta fractionation in peraluminous granites: A marker of the magmatic-hydrothermal transition', Geology, 44(3), pp. 231–234. https://doi.org/10.1130/g37475.1.
Lehmann, B. (1990) Metallogeny of Tin. Springer-Verlag. https://doi.org/10.1007/bfb0010922.
Lehmann, B. (2020) 'Formation of tin ore deposits: A reassessment', Lithos, p. 105756. https://doi.org/10.1016/j.lithos.2020.105756.
Nassar, N.T., Graedel, T.E. and Harper, E.M. (2015) 'By-product metals are technologically essential but have problematic supply', Science advances, 1(3), https://doi.org/10.1126/sciadv.1400180.
Skirrow, R.G. et al. (2013) Critical commodities for a high-tech world: Australia"s potential to supply global demand. Canberra: Geoscience Australia, pp. 1–118. http://pid.geoscience.gov.au/dataset/ga/76526.
Taylor, R.G. (1979) Geology of Tin Deposits. Elsevier Science.

https://www.cet.edu.au/

Centre for EXPLORATION TARGETING